Imaging currents in HgTe quantum wells in the quantum spin Hall regime

Katja C. Nowack[2,3*], Eric M. Spanton[1,3], Matthias Baenninger[1,3], Markus König[1,3], John R. Kirtley[2], Beena Kalisky[2,4], C. Ames[5], Philipp Leubner[5], Christoph Brüne[5], Hartmut Buhmann[5], Laurens W. Molenkamp[5], David Goldhaber-Gordon[1,3], Kathryn A. Moler[1,2,3]

[1]Department of Physics, Stanford University, Stanford, California 94305, USA

[2]Department of Applied Physics, Stanford University, Stanford, California 94305, USA

[3]Stanford Institute for Materials and Energy Sciences, SLAC National Accelerator Laboratory, Menlo Park, California 94025, USA

[4]Department of Physics, Nano-magnetism Research Center, Institute of Nanotechnology and Advanced Materials, Bar-Ilan University, Ramat-Gan 52900, Israel.

[5]Physikalisches Institut (EP3), Universität Würzburg, Am Hubland, D-97074, Würzburg, Germany

*Email: knowack@stanford.edu

The quantum spin Hall (QSH) state is a state of matter characterized by a non-trivial topology of its band structure, and associated conducting edge channels[1-5]. The QSH state was predicted[6] and experimentally demonstrated[7] to be realized in HgTe quantum wells. The existence of the edge channels has been inferred from local and non-local transport measurements in sufficiently small devices[7-9]. Here we directly confirm the existence of the edge channels by imaging the magnetic fields produced by current flowing in large Hall bars made from HgTe quantum wells. These images distinguish between current that passes through each edge and the bulk. Upon tuning the bulk conductivity by gating or raising the temperature, we observe a regime in which the edge channels clearly coexist

Work supported by US Department of Energy contract DE-AC02-76SF00515 and BES.

with the conducting bulk, providing input to the question of how ballistic transport may be limited in the edge channels. Our results represent a versatile method for characterization of new quantum spin Hall materials systems[10-13].

Like an ordinary insulator, the QSH state has a bulk energy gap, but the QSH state supports within the gap a pair of counter-propagating spin-polarized edge modes [1-5]. The QSH state is predicted in HgTe/(Hg,Cd)Te quantum wells thicker than a critical thickness of 6.3 nm, whereas thinner quantum wells should be ordinary insulators[6,7]. The edge modes are theoretically protected against backscattering by their orthogonal spin states[14-16], and therefore should have a quantized conductance of e^2/h, where e is the charge of an electron and h is Planck's constant. Experimentally, nearly-quantized conductance[7,8,17] as well as transport signatures of the spin polarization[9] have been found only in devices with edges of several microns or shorter. For larger devices, the measured resistances deviate from the values expected for dissipationless edge channels[7,8,17]. The ballistic nature of the edge channels could be affected by spatially-varying quantum well thickness or doping[8,18,19], magnetic[20] or non-magnetic impurities[21], or Rashba spin-orbit interaction combined with either electron-electron interactions[22] or phonons[23]. Inelastic scattering processes are a common ingredient in these scenarios, in some cases associated with the presence of bulk states whose coupling to the edge channels is experimentally still relatively unexplored.

To confirm the presence of the edge channels and study their interplay with a conducting bulk, we image the magnetic field produced by the current through large Hall bars with a scanning superconducting quantum interference device[24] (SQUID, Fig. 1a) from which we reconstruct the current density with several micron spatial resolution (see below). All images and profiles are

normalized to the applied current. Although most scanning probes cannot image through the top gates which are usually used to tune carrier density, our technique can.

Hall bars with lateral dimensions as shown in Fig. 1b are fabricated from HgTe/(Hg,Cd)Te quantum well structures with well thicknesses (6.6 nm for H1, 8.5 nm for H2 determined by X-ray reflectivity) above the critical thickness[25]. We use only the upper two contacts of the Hall bars to avoid the SQUID touching wire bonds. The two-terminal resistance R_{2T} of H1 is shown in Fig. 1c. We also measured a Hall bar, H3, with a quantum well thinner than the critical thickness (5 nm). Measurements are done at $T \sim 3$ K unless noted differently.

Fig. 1d and e summarize our main result. When the transport is dominated by bulk conduction (Fig. 1d), the magnetic profile crosses smoothly through zero in the Hall bar, corresponding to homogeneous current flow through the Hall bar. In clear contrast, when the transport is dominated by edge channels (Fig. 1e), the magnetic profile displays two steep crossings through zero at the top and bottom edge of the Hall bar, showing that the current predominantly flows along the edge of the device. The width of features is limited by our spatial resolution (see below). The current along the lower edge fully traces out the perimeter of the top gated part of the Hall bar.

For a two-dimensional current density there is a one-to-one correspondence via the Biot-Savart law between the current density and the *z*-component of the magnetic field produced by the current[26]. Since the current density in the Hall bar is two-dimensional we can therefore directly obtain it (Fig. 1 f-i) from our magnetic images, which are a convolution of the *z*-component of the magnetic field with the SQUID pickup loop. We implement the reconstruction using Fourier

transforms[26] and the geometry of the pickup loop as deduced from images of isolated vortices in a bulk superconductor, which act as near-ideal monopole field sources (Supplementary Information). Fig. 1g and i clearly show that the current flows along the edges of the gated part of the Hall bar, while it spreads out in the ungated parts and the contacts. These current images directly confirm the existence of edge channels in the QSH regime.

The width of the features in the reconstructed current densities is limited by the 3 μm diameter pickup loop and its scan height of 1.5-2 μm. Systematic errors in the inversion such as ringing and finite current density outside the boundary of the Hall bar result from uncertainty in scan height, imperfect characterization of the pickup loop, noise, and the finite image size (Supplementary Information). All results presented here are qualitatively robust against these systematic errors.

Having compared the extreme cases of bulk- and edge-dominated transport at low and maximum R_{2T}, respectively, we next explore the interplay between them. The top gate voltage, V_{TG}, tunes the Fermi level from the valence band through the bulk energy gap into the conduction band and thereby changes the bulk conductance, with the bulk being insulating when the Fermi level is in the gap. For a range of V_{TG}, we find that edge conduction coexists with bulk conduction (Fig. 2 a-d). In Fig. 2e we show the percentage of current flowing along the edges and bulk obtained by modelling the current profiles shown in Fig. 2c,d and profiles at additional values of V_{TG} as a sum of three contributions (Fig. 2f) determined where either the bulk or the edges clearly dominate. The errors are difficult to evaluate (Supplementary Information), but we can identify the presence of a distinct edge current even when the edge carries an order of magnitude less total current than the bulk. Qualitatively, we find that the current flow changes

gradually from edge-dominated to bulk-dominated when moving away from the maximum in R_{2T}, with a large region of coexistence of edge channels and bulk conduction.

If the bulk and the edges were three uncoupled parallel resistors, we would be able to calculate their resistances by dividing R_{2T} by the respective current percentage. In Figure 2g we plot the effective resistances of the top edge and bulk obtained from this model, omitting the resistance of the bottom edge from the figure for clarity. The bulk resistance resembles an insulator with steep flanks as a function of V_{TG}. Interestingly, the resistance of the top edge is rather flat for the V_{TG} range at which it is lower or comparable to the bulk resistance.

So far, the coupling between the edges and the bulk is largely unexplored, both theoretically and experimentally. It is outside the scope of this work to establish a model for their interplay; however, the observation of their coexistence and the effective resistance may provide input into models of their coupling. Possible relevant factors include a mismatch in k-space between the edge and the bulk states and the formation of a depletion region where the edge channel is laterally localized.

Comparing the top and bottom paths provides additional information. The bottom path has several edge segments separated by contacts and ungated parts of the Hall bar which have a low resistance (based on R_{2T} at V_{TG} = 0 V) and therefore should act like contacts. If the edge channels were fully ballistic, each edge segment would contribute h/e^2 to the resistance[8]. Hence, the top and bottom path would have resistances of h/e^2 and $5h/e^2$ respectively, a ratio of 1:5. However, the maximum R_{2T} ~200 kΩ >> h/e^2 reveals that the edge channels are not ballistic over their full length, as is typical for this size device [7,17]. In the case of fully diffusive edges, the ratio is expected to be 1:1.6 based on the path lengths, expecting that the resistance of the ungated segments is negligible compared to the bottom path. H1 and H2 showed ratios close to

1:8 and 1:1 respectively between the bottom and top edge current (Fig. 2e and 3c). These results are consistent with ballistic segments of edge channels of several microns length, interrupted by scattering sites[8] whose location and number are expected to be random and to vary between samples.

Other factors may also affect the variability between H1 and H2. For example, the difference in quantum well thickness and substrate (Supplementary Information) and hence band structure between H1 and H2 and the slight difference in temperature (3K for H1, 4K for H2) causes more residual bulk conduction in H2 at maximum R_{2T}. When R_{2T} decreases in H1, the percentage of current along the bottom edge initially increases (Fig. 2e). This occurs because more current arrives at the bottom edge through the bulk of the device.

The profiles shown in Fig. 2 correspond to a fixed x-position along the Hall bar. However, at values of V_{TG} corresponding to the flanks of the resistance peak the amount of current flowing along the edge changes along the Hall bar and some inhomogeneity is present (see Supplementary Information for images). This could be caused by disordered charge in the gate dielectric, inhomogeneous capacitive coupling of the gate to the Hall bar, disorder in the doping layer or inhomogeneity of the quantum well thickness.

In a different thermal cycle of H1, we observed pronounced inhomogeneity, which we believe was caused by inhomogeneous charge in the gate dielectric originating from an unintentional electrical shock of the top gate. Remarkably, R_{2T} was significantly lower, but still displaying a peak that could falsely be interpreted as originating from a closer to ideal edge channel. However, imaging reveals that inhomogeneity over tens of microns causes the bulk to remain conductive in parts of the Hall bar at every V_{TG}, and that each region of the Hall bar shows well-

defined edge conduction at some V_{TG} (see Supplementary Information for R_{2T} and images) exemplifying how imaging can be used as a diagnostic tool complementary to transport.

To further study the robustness of the edge conduction and its coexistence with a conducting bulk, we test how temperature affects the current distribution in H2 (Fig. 3a). The maximum R_{2T} decreases with increasing temperature (Fig. 3b) and the corresponding magnetic profiles show increased bulk conduction. We extract the percentages of edge and bulk current (Fig. 3c) by directly fitting the magnetic profiles (Supplementary Information) and find effective resistances for the top edge, bottom edge, and bulk as described above. The edge resistance is rather temperature independent while the bulk resistance drops steeply with temperature (Fig. 3d), consistent with thermally activated conduction.

Possible trivial origins for pronounced edge conduction include doping of the edges during fabrication and related band bending. To address this issue, we imaged the current flow in a Hall bar made from a 5 nm thick quantum well. When gated this device shows, as expected, insulating behaviour (Fig. 4a). Our method does not allow us to image the device when it is fully insulating, since we cannot pass a current through. However, we imaged the device up to a resistance that is significantly higher than the maximum R_{2T} of H1 and H2 (Fig. 4 b-d). We have found no signatures of enhanced conduction along the edge.

The evidence for helical edge channels from transport measurements[7-9], the absence of edge currents in the 5 nm wide quantum well, and the presence of edge current throughout the full resistance peak in the Hall bars with thicknesses above the critical thickness all indicate that our observations originate from the QSH effect.

In conclusion, we directly demonstrate through images the presence of edge channels in HgTe quantum wells in the QSH regime. We observe that edge channels dominate the transport even when the device edges are much longer than the scattering length and that the edge channels persist in the presence of bulk conduction. These properties of the edge channels will need to be explained by any theories of the mechanisms that limit ballistic transport, and would be challenging to establish with global transport measurements alone.

Reducing the size of our sensor, bringing it closer to the device and more carefully characterizing its point spread function will significantly improve the spatial resolution in future experiments. Our technique is non-invasive and compatible with the use of a top gate. Our results open the way to explore other topologically non-trivial materials[10-13] with a combination of global transport and local imaging.

Methods Summary

Hall bars H1, H2 and H3 were fabricated from two different HgTe/(Hg,Cd)Te quantum well structures with well thickness of 6.6 nm, 8.5 nm and 5 nm (see Supplementary Information). The devices were patterned using optical lithography and subsequent Ar ion-beam etching[25]. The top gates were also patterned using optical lithography and consist of a 40 nm-thick Al_2O_3 gate insulator and a Ti (5 nm)/Au (50 nm) gate electrode (see Supplementary Information).

All presented images were taken by applying an AC current to the Hall bars and recording the SQUID signal using a lock-in amplifier. The SQUID signal is directly proportional to the flux in the pickup loop caused by the *z*-component of the magnetic field generated by the current. We normalize the measured flux to the applied current, which results in units Φ_0/A for the magnetic

images and profiles, where Φ_0 is the magnetic flux quantum. The magnetic images and profiles in Fig. 1-3 were taken at an rms current amplitude ranging from 100 nA to 500 nA (apart from the profile at V_{TG} = 0.1V in Fig. 2, which was taken at 1 μA). Magnetic images in Fig. 4 were taken at an rms current ranging from 80 nA to 190 nA (additional images with ~15 nA applied were taken yielding the same results). For some images, this corresponds to bias voltages that are higher than typically applied in transport experiments. We have explicitly checked that all shown measurements were recorded in or close to the linear regime (Supplementary Information).

References

1. Kane, C. L. & Mele, E. J. Quantum spin Hall effect in graphene. *Phys. Rev. Lett.* **95**, 226801 (2005).
2. Bernevig, B. A. & Zhang, S.-C. Quantum spin Hall effect. *Phys. Rev. Lett.* **96**, 106802 (2006).
3. Kane, C. L. & Mele, E. J. Z_2 Topological order and the quantum spin Hall effect. *Phys. Rev. Lett.* **95**, 146802 (2005).
4. Qi, X.-L. & Zhang, S.-C. Topological insulators and superconductors. *Rev. Mod. Phys.* **83**, 1057–1110 (2011).
5. Hasan, M. Z. & Kane, C. L. Colloquium: Topological insulators. *Rev. Mod. Phys.* **82**, 3045–3067 (2010).
6. Bernevig, B. A., Hughes, T. L. & Zhang, S.-C. Quantum spin Hall effect and topological phase transition in HgTe quantum wells. *Science* **314**, 1757–1761 (2006).
7. König, M. *et al.* Quantum spin Hall insulator state in HgTe quantum wells. *Science* **318**, 766–770 (2007).
8. Roth, A. *et al.* Nonlocal transport in the quantum spin Hall state. *Science* **325**, 294–297 (2009).
9. Brüne, C. *et al.* Spin polarization of the quantum spin Hall edge states. *Nature Physics* **8**, 485–490 (2012).
10. Murakami, S. Quantum spin Hall effect and enhanced magnetic response by spin-orbit coupling. *Phys. Rev. Lett.* **97**, 236805 (2006).
11. Shitade, A. *et al.* Quantum spin Hall effect in a transition metal oxide Na_2IrO_3. *Phys. Rev. Lett.* **102**, 256403 (2009).
12. Liu, C.-X. *et al.* Oscillatory crossover from two-dimensional to three-dimensional topological insulators. *Phys. Rev. B* **81**, 041307 (2010).
13. Knez, I., Du, R. R. & Sullivan, G. Evidence for helical edge modes in inverted InAs/GaSb quantum wells. *Phys. Rev. Lett.* **107**, 136603 (2011).
14. Wu, C., Bernevig, B. A. & Zhang, S.-C. Helical liquid and the edge of quantum spin Hall systems. *Phys. Rev. Lett.* **96**, 106401 (2006).

15. Xu, C. & Moore, J. E. Stability of the quantum spin Hall effect: Effects of interactions, disorder, and Z2 topology. *Phys. Rev. B* **73**, 045322 (2006).
16. Delplace, P., Li, J. & Büttiker, M. Magnetic-field-induced localization in 2D topological insulators. *Phys. Rev. Lett.* **109**, 246803 (2012).
17. König, M. *et al.* The quantum spin Hall effect: Theory and experiment. *J. Phys. Soc. Jpn.* **77**, 031007 (2008).
18. Maciejko, J., Qi, X.-L. & Zhang, S.-C. Magnetoconductance of the quantum spin Hall state. *Phys. Rev. B* **82**, 155310 (2010).
19. Väyrynen, J. I., Goldstein, M. & Glazman, L. I. Helical edge resistance introduced by charge puddles. *arxiv:1303.1766.*
20. Maciejko, J. *et al.* Kondo effect in the helical edge liquid of the quantum spin Hall state. *Phys. Rev. Lett.* **102**, 256803 (2009).
21. Schmidt, T. L., Rachel, S., Oppen, von, F. & Glazman, L. I. Inelastic electron backscattering in a generic helical edge channel. *Phys. Rev. Lett.* **108**, 156402 (2012).
22. Väyrynen, J. I. & Ojanen, T. Electrical manipulation and measurement of spin properties of quantum spin Hall edge states. *Phys. Rev. Lett.* **106**, 076803 (2011).
23. Budich, J. C., Dolcini, F., Recher, P. & Trauzettel, B. Phonon-induced backscattering in helical edge states. *Phys. Rev. Lett.* **108**, 086602 (2012).
24. Huber, M. E. *et al.* Gradiometric micro-SQUID susceptometer for scanning measurements of mesoscopic samples. *Rev. Sci. Instrum.* **79**, 053704 (2008).
25. Baenninger, M. *et al.* Fabrication of samples for scanning probe experiments on quantum spin Hall effect in HgTe quantum wells. *Journal of Applied Physics* **112**, 103713 (2012).
26. Roth, B. J., Sepulveda, N. G. & Wikswo, J. P. Using a magnetometer to image a two-dimensional current distribution. *Journal of Applied Physics* **65**, 361–372 (1989).
27. König, M. *et al.* Spatially resolved study of backscattering in the quantum spin Hall state. *Phys. Rev. X* **3**, 021003 (2013).
28. Ma, Y. *et al.* Direct imaging of quantum spin Hall edge states in HgTe quantum well. *arxiv:1212.6441*.

Supplementary Information is linked to the online version of the paper.

Acknowledgements

We thank S. C. Zhang, X. L. Qi, M. R. Calvo for valuable discussions, J. A. Bert and H. Noad for assistance with the experiment, G. Stewart for rendering Fig. 1a and M. E. Huber for assistance in SQUID design and fabrication. This work was funded by the Department of Energy, Office of Basic Energy Sciences, Division of Materials Sciences and Engineering, under contract DE-AC02- 76SF00515 (Sample fabrication and scanning SQUID imaging of the QSH state in HgTe Hall bars), by the DARPA Meso project under grant no. N66001-11-1-4105 (MBE growth of the HgTe heterostructures) and by the Center for Probing the Nanoscale, an

NSF NSEC, supported under grant no. PHY-0830228 (development of the scanning SQUID technique). The work at Würzburg was also supported by the German research foundation DFG (SPP 1285 'Halbleiter Spintronik' and DFG-JST joint research program 'Topological Electronics') and by the EU through the ERC-AG program (project '3-TOP'). B.K. acknowledges support from FENA.

Some of the present authors are involved in two other complementary scanning probe measurements on HgTe/(Hg,Cd)Te quantum wells, performed in parallel with this one, including one using scanning gate microscopy that identifies localized scattering sites along the edge[27], and one using scanning microwave impedance microscopy to image the local conductivity[28].

Author Contributions

K. C. N. and E. M. S. performed the SQUID measurements. K. C. N., E. M. S., B. K., J. R. K analysed the results with input from K. A. M., D. G. G., M. K. , M. B.. M. B. fabricated the samples. C. A., P. L., C. B., H. B. and L. W. M. grew the quantum well structures. K. A. M., D. G. G. and L. W. M. guided the work. K. C. N. and K. A. M. wrote the manuscript with input from all co-authors.

Additional Information

Supplementary information is available in the online version of the paper. Reprints and permissions information is available online at www.nature.com/reprints. Correspondence and requests for materials should be addressed to K. C. N.

Competing financial interests

The authors declare no competing financial interests.

Figure Captions

Figure 1. Current flows along the edge in the QSH regime. a, Sketch of the measurement. The magnetic field (red) generated by the current (blue) is measured by detecting the flux through the SQUID's pickup loop. **b,** Schematic of the Hall bar. **c,** Two terminal resistance R_{2T} of H1 vs. top gate voltage V_{TG}. **d, e,** Magnetic images at V_{TG} as indicated in **c** measured on H1. In **d** a 20 μm scalebar (black), the outline of the Hall bar mesa (white dashed line) and a sketch of the pickup loop (black) are included; grey arrow indicates the *x*-position of the profiles in Fig. 2. In **e** an outline of the top gate (grey dashed line) is included. **f, g,** *X*-component and **h,i,** *y*-component of the two-dimensional current density obtained from the current inversion of the magnetic images in **d** and **e** respectively. The magnetic images and the current densities are normalized to the applied current.

Figure 2. Coexistence of edge channels and a conducting bulk. a, b, Magnetic profiles along the *y*-direction at the position as indicated in Fig. 1d as a function of V_{TG}. Insets: R_{2T} from Fig. 1b, dot colours match the profile colours to indicate V_{TG}. **c, d,** Current profiles at the same position and with the same colour coding as in **a, b**. All line cuts are averaged over a width of ~ 2 μm. Integration of the current profiles given in rescaled units μm^{-1} yields 1.0 +/- 0.05, as expected. **e,** Percentage of current flowing along the top edge (blue crosses), the bottom edge (green circles) and through the bulk (red diamonds) obtained through modelling each current profile in **c, d** by a sum of a bulk and two edge contributions as sketched in **f**, where amplitudes F_{top}, F_{bulk} and F_{bottom} give the current percentage. **g,** Effective resistances of the bulk (symbols and colours as in **e**) and the top edge obtained from dividing the two-terminal resistance R_{2T} by

the current fractions from **e** at each V_{TG}. V_{TG} is restricted to values at which $F_{top} > 10\%$. Grey lines in **e** and **g** are R_{2T} from Fig. 1c in a.u.

Figure 3. Temperature dependence. a, Magnetic profiles as a function of temperature measured on Hall bar H2. V_{TG} is adjusted for each profile, such that R_{2T} is at its maximum. **b,** Maximum value of R_{2T} as a function of temperature. **c,** Percentage of current flowing along the top and bottom edge and through the bulk, extracted from fitting the magnetic profiles in **a** with a bulk and two edge contributions. **d,** Effective resistance of the bulk and the edges obtained from dividing R_{2T} by the current percentage.

Figure 4. No signatures of edge conduction in quantum well thinner than the critical thickness. a, Two terminal resistance of H3 (quantum well thinner than the critical thickness). The resistance of the device exceeds several tens of MΩ. **b-e,** Magnetic images at top gate voltages as indicated in **a**. 20 μm scalebar is shown in **b**.

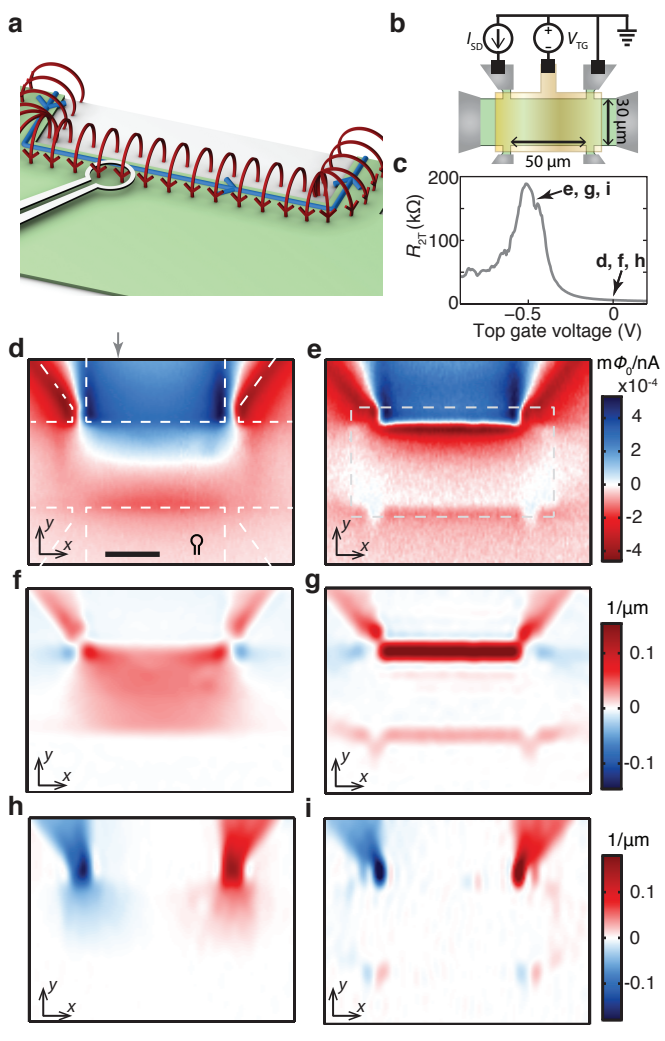
a
b
I_{SD}
V_{TG}
30 µm
50 µm
c
200
100
0
R_{2T} (kΩ)
e, g, i
d, f, h
−0.5
0
Top gate voltage (V)
d
e
mΦ0/nA
x10-4
4
2
0
-2
-4
y
x
f
g
1/µm
0.1
0
-0.1
h
i

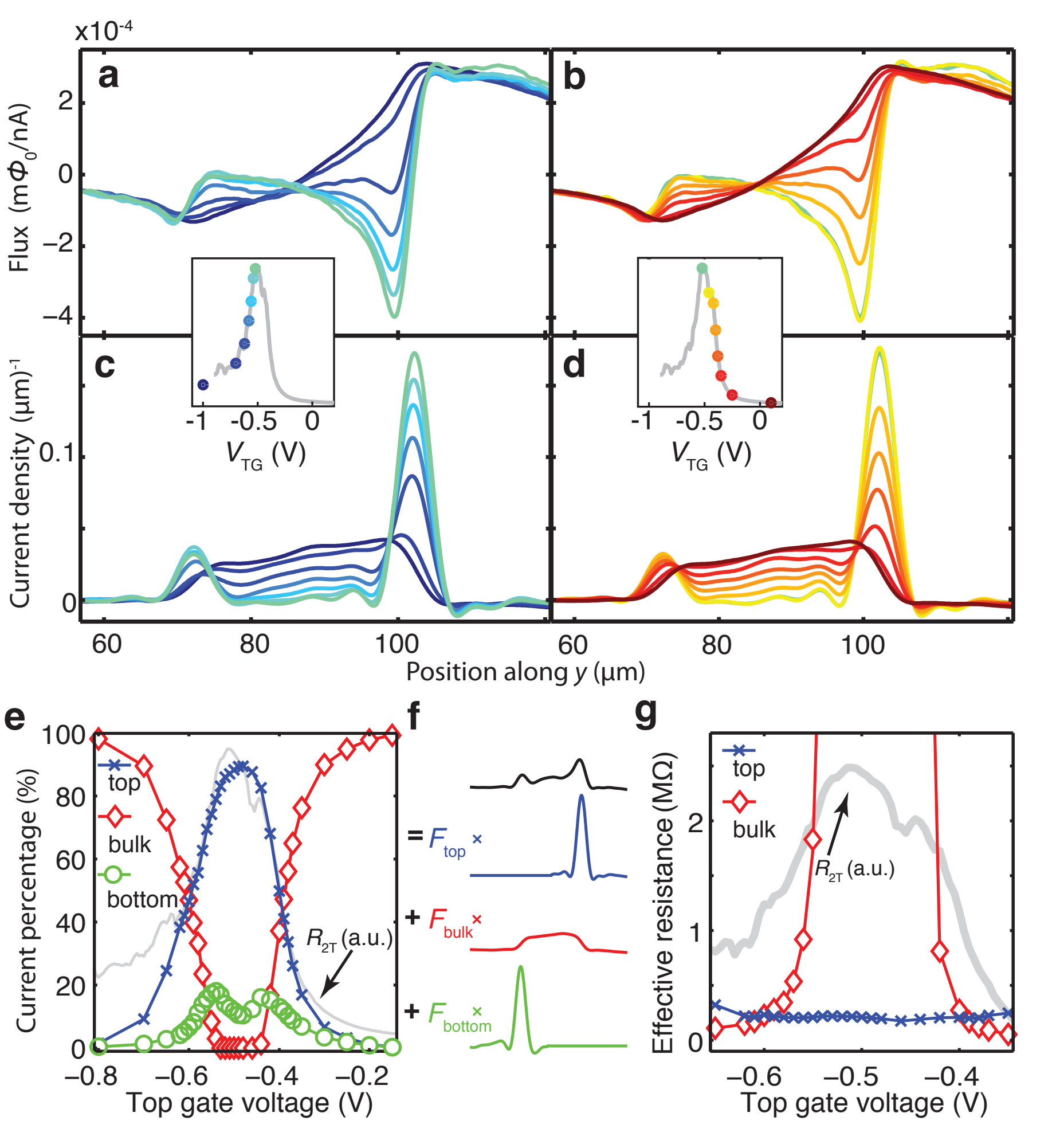
x10-4
a
b
c
d
Flux (mΦ0/nA)
Current density (μm)-1
VTG (V)
Position along y (μm)
e
f
g
top
bulk
bottom
R2T (a.u.)
Current percentage (%)
Top gate voltage (V)
= Ftop ×
+ Fbulk ×
+ Fbottom ×
Effective resistance (MΩ)

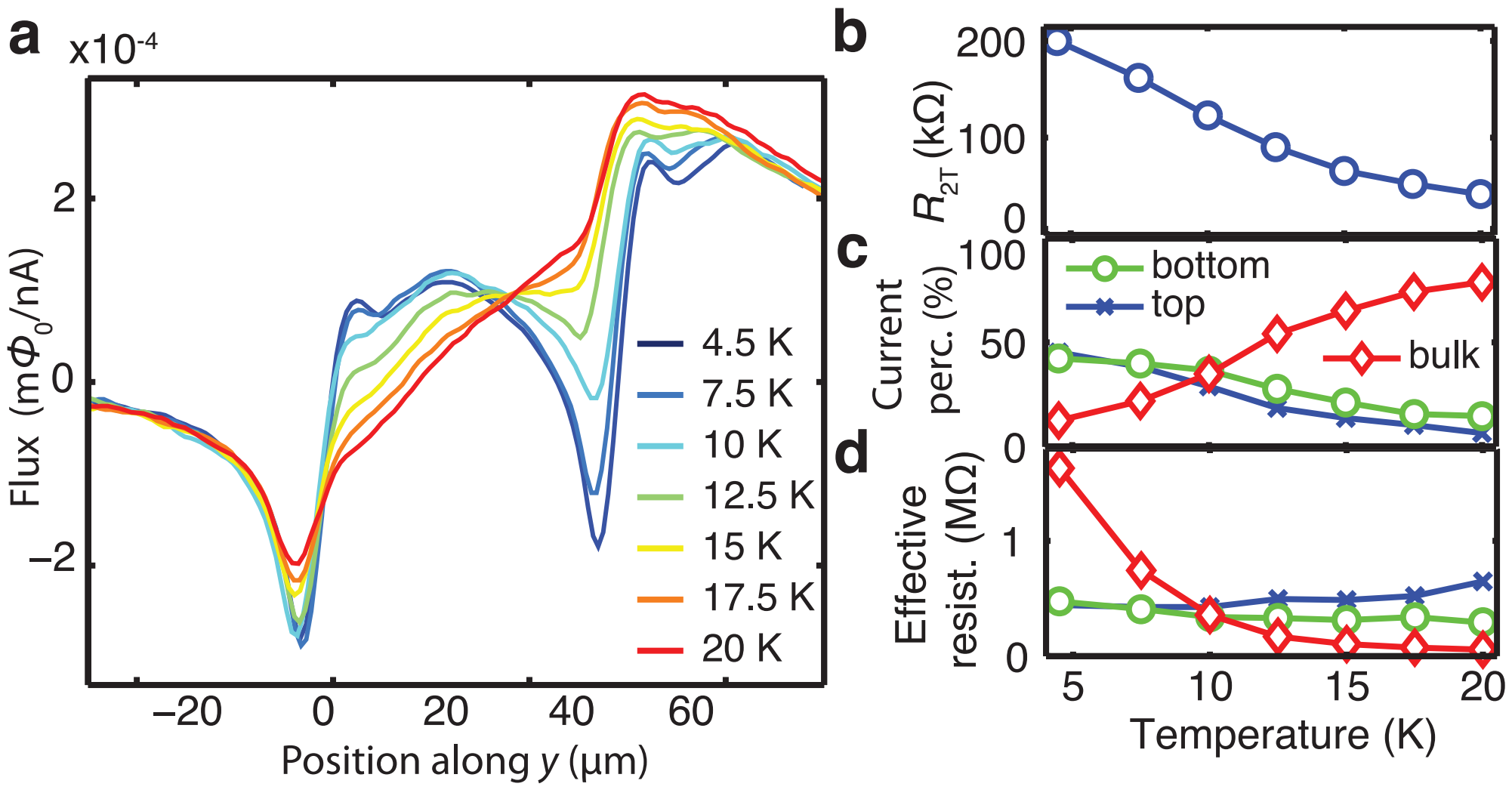
a
x10-4
2
0
−2
Flux (mΦ0/nA)
−20
0
20
40
60
Position along y (μm)
4.5 K
7.5 K
10 K
12.5 K
15 K
17.5 K
20 K
b
200
100
0
R2T (kΩ)
c
100
50
0
Current perc. (%)
bottom
top
bulk
d
1
0
Effective resist. (MΩ)
5
10
15
20
Temperature (K)

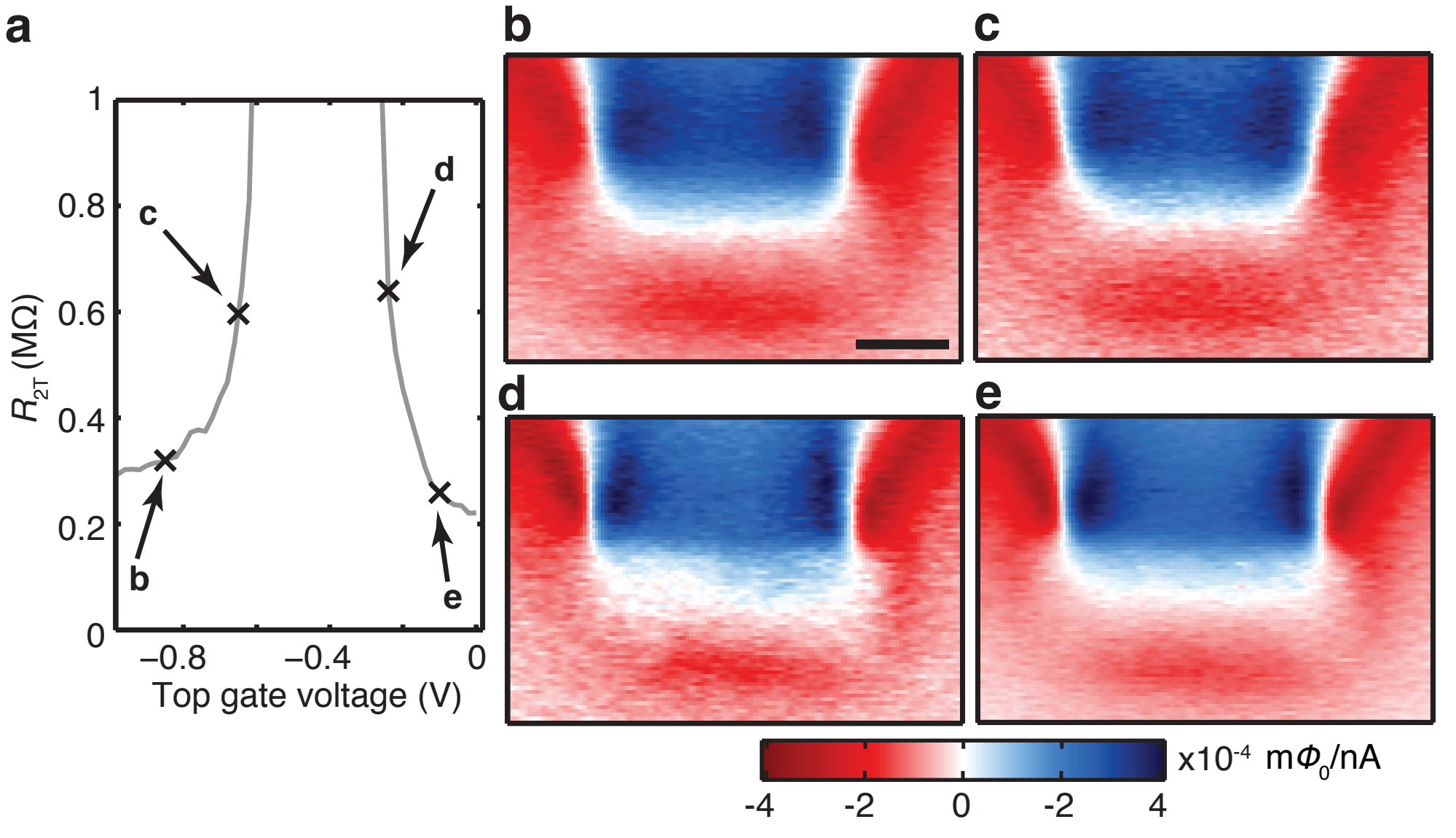
a
b
c
d
e
1
0.8
0.6
0.4
0.2
0
R_{2T} (MΩ)
–0.8
–0.4
0
Top gate voltage (V)
x10^{-4} mΦ_0/nA
-4
-2
0
-2
4